Inorganic Chemistry Communications 93 (2018) 42–46

Contents lists available at ScienceDirect

Inorganic Chemistry Communications

journal homepage: www.elsevier.com/locate/inoche

Short communication

Semiconductive 1D nanobelt iodoplumbate hybrid with high humidity response

MinLan Cai[a,b], Guan-E Wang[a,*], MingShui Yao[a], GuoDong Wu[a], Ying Li[c], Gang Xu[a]

[a] State Key Laboratory of Structural Chemistry, Fujian Institute of Research on the Structure of Matter, Chinese Academy of Sciences, Fuzhou, Fujian 350002, PR China
[b] Fujian Key Laboratory of Polymer Materials, College of Chemistry and Materials Science, Fujian Normal University, Fuzhou, Fujian 350007, PR China
[c] State Key Laboratory of Safety and Control for Chemicals, SINOPEC R Research Institute of Safety Engineering, Qingdao, Shandong 266101, PR China

GRAPHICAL ABSTRACT

A new compound, $[(Et_2)HDABH(Et_2)]_2Pb_5I_{14}\cdot 2H_2O$ (DAB = benzidine), has been solvothermally synthesized. It exhibits unusual one-dimensional (1D) nanobelt structure. The compound presents typical semiconductive behavior, whose conductivity increases along with the raising of temperature. Moreover, the compound shows more than 4 orders of magnitude resistance response to 90% RH.

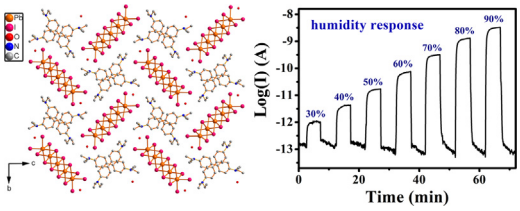

ARTICLE INFO

Keywords:
Functional motifs
Inorganic-organic hybrid
Nanobelt
Semiconductor
Sensor

ABSTRACT

Owing to the structural diversity and potential applications in optoelectronic devices, inorganic-organic hybrid materials have attracted extensive attentions in recent years. They are widely used in the fields of fluorescence, photoconductivity, ferroelectricity and solar cells. A new compound, $[(Et_2)HDABH(Et_2)]_2Pb_5I_{14}\cdot 2H_2O$ (DAB = benzidine), was solvothermally synthesized using $[(Et_2)HDABH(Et_2)]^{2+}$ as templates and balance cations. The structure is consisted of one-dimensional (1D) nanobelt iodoplumbate, $[(Et_2)HDABH(Et_2)]^{2+}$ dications and water molecules. The compound exhibits typical semiconductive behaviors, whose conductivity increases along with the raising of temperature. The compound also shows high electrical response to humidity, which indicates great potential application in humidity quantitatively detecting.

1. Introduction

The structural flexibility and tunability of metal halide based inorganic-organic hybrid materials provide a fertile possibility for the preparation of fascinating crystal structures with various physical properties. Especially, electrical performance is closely related to the dimension of materials. For example, the diamond, graphene, and carbon nanotube, which consist of carbon element, with three-dimensional (3D) diamond structure, two-dimensional (2D) layers and 1D nanotubes, respectively, exhibit very different electrical properties. The diamond is an insulator, whereas graphene has metallic conductive properties. Furthermore, tailoring the graphene to graphene nanoribbons (GNR) will change their conductive properties to semiconductive character [1]. Inspired by these results, metal halide based inorganic-organic hybrid material with 1D nanobelt structure may display different properties from 3D or 2D structures, but is rarely reported.

Metal halide inorganic-organic hybrids as a kind of promising semiconductor material, have gained much attention for their potential applications in optoelectronic devices [2]. (Pyrrolidinium)$MnCl_3$ [3] and (3-Pyrrolinium)$MnCl_3$ [4], reported by Xiong et al., exhibit high efficient red-light emission and excellent ferroelectricity

* Corresponding author at: 155 Yangqiao West Road, Fuzhou, Fujian 350002, PR China.
E-mail address: gewang@fjirsm.ac.cn (G.-E. Wang).

https://doi.org/10.1016/j.inoche.2018.05.002
Received 13 April 2018; Received in revised form 28 April 2018; Accepted 2 May 2018
Available online 03 May 2018
1387-7003/

properties, which may extend the application of hybrid perovskites to the field of ferroelectric luminescence or multifunctional devices. Solar cell devices which fabricated with this hybrid material, $(CH_3NH_3)PbX_3$ (X = Cl, Br, I), show power conversion efficiency increases from 3.8% to higher than 20% within only a few years [5]. In this hybrid, the inorganic parts are the functional motifs for electrical conduction [6], because the semiconductive properties of the hybrids are largely depended on the structure of inorganic anions: The calculated resistivity value for a single-crystal of $CH_3NH_3PbI_3$ with 3D perovskite structure is 51 MΩ cm at room temperature [7]; The conductivities of $(H_2DABCO)(Pb_2Cl_6)$ and $(H_3O)(Et_2\text{-}DABCO)_8(Pb_{21}Cl_{59})$ with different 3D inorganic frameworks are 2.18×10^{-7} S cm^{-1} and 2.83×10^{-7} S cm^{-1}, respectively [8]; The conductivity of 2D multi-layered hybrid perovskite $(C_4H_9NH_3)_2(CH_3NH_3)_2Pb_3Br_{10}$ is about 10^{-10} S cm^{-1} [9]; $(C_4H_9NH_3)_2(CH_3NH_3)_{n-1}Sn_nI_{3n+1}$ with 2D layered structure shows a transition from semiconducting to metallic behavior with increasing the number of perovskite layers [10]; The conductivity of $[Pb^{II}_{18}I_{54}(I_2)_9]$ nanotube is 0.9×10^{-10} S cm^{-1} perpendicular to the nanotube and 0.8×10^{-9} S cm^{-1} along the nanotube, respectively [11]. These results indicate that the conductivity of the hybrids is closely related to their structures. Furthermore, metal halide based inorganic-organic hybrids, especially the lead halide based family, exhibits a wide variety of structure types due to the flexibility of the Pb(II) coordination polyhedron and the templating effect of the cations [12]. However, remarkable progresses in inorganic-organic hybrids are mainly focus on 3D and 2D structures, low dimensional structures are significantly underexplored [13]. The conductivity of 1D nanobelt iodioplumbate chain has not been investigated, but is extremely desired for their further application.

Herein, we demonstrate one-step solvothermal syntheses of a new iodoplumbate hybrid material, $[(Et_2)HDABH(Et_2)]_2Pb_5I_{14}{\cdot}2H_2O$ (**1**), which contains a novel 1D nanobelt iodioplumbate chain as the inorganic component. Compound **1** shows semiconducting properties and high electrical response to humidity.

2. Experimental section

2.1. Synthesis and crystal growth

PbI_2, benzidine (DAB), HI, and ethanol were received from Sinopharm Chemical Reagent Co. Ltd. They were directly used without further purification. A mixture of PbI_2 (0.231 g, 0.25 mmol), DAB (0.092 g, 0.5 mmol), ethanol (5 mL) and concentrated HI (1.5 mL, 45%) was heated at 150 °C for 3 days in a sealed 25 mL Teflon-lined stainless steel vessel. Upon cooling to room temperature at a rate of 2.5 °C h^{-1}, yellow prism crystals of **1** were obtained in 82% yield (based on PbI_2). The purity of the mechanical separation sample is proved by the powder X-ray diffraction (Fig. S1) and elemental analysis. Elem. Anal. Calcd. For $[(Et_2)HDABH(Et_2)]_2Pb_5I_{14}{\cdot}2H_2O$ (%): C: 9.05, H: 0.75, N: 1.76. Found: C: 9.24, H: 0.77, N: 1.78. ^{1}H NMR (400 MHz, DMSO-d_6) δ 8.03 (s, 4H), 7.78 (d, J = 8.4 Hz, 4H), 3.43–3.76 (m, 8H), 1.117 (t, J = 7.2 Hz, 12H). IR (KBr, cm^{-1}): 2975 (w), 2933 (w), 2881 (w), 2686 (w), 2642 (w), 1594 (m), 1489 (s), 1436 (m), 1374 (m), 1264 (w), 1179 (w), 1143 (m), 1100 (m), 1000 (s), 807 (s), 712 (w), 639 (w), 539 (s).

2.2. Single crystal X-ray diffraction

The single crystal X-ray diffraction measurement was performed on a Rigaku Ultrax-Saturn 70 diffractometer using graphite-monochromated Mo-K_α radiation (λ = 0.71073 Å). Intensity data set was collected using an ω scan technique and corrected for Lp effects. The primitive structure was solved by the direct method using the Siemens SHELXTL™ Version 5 package of crystallographic software. The difference Fourier maps based on these atomic positions yield the other non-hydrogen atoms. The final structure was refined using a full-matrix least-squares refinement on F^2. All non-hydrogen atoms were refined anisotropically. Hydrogen atoms on carbon, nitrogen and oxygen atoms were generated geometrically. Crystallographic data has been deposited with the Cambridge Crystallographic Data Centre: CCDC 1573042. This data can be obtained free of charge from The Cambridge Crystallographic Data Center *via* www.ccdc.cam.ac.uk/data_request/cif. Additional crystallographic details are given in Table 1, and the bond distances and angles are given in Tables 2 and 3.

Table 1
Crystal and structure refinement data for **1**.

1	
Formula	$[(Et_2)HDABH(Et_2)]_2Pb_5I_{14}{\cdot}2H_2O$
Color and habit	Yellow prism
Crystal size (mm)	0.20 × 0.08 × 0.08
Space group	$P2_1c$
a (Å)	7.903(1)
b (Å)	19.902(2)
c (Å)	24.102(3)
α (°)	90
β (°)	96.546(9)
γ (°)	90
V (Å^3)	3765.9(7)
Z	2
Formula weight	3441.47
ρ_{calcd} (g cm^{-3})	3.035
μ (mm^{-1})	16.908
F(000)	2992
θ (°)	2.59 to 25.50
Completeness	98.7%
Reflections measured	24,300
Indep. reflections (R_{int})	6913[$R_{(int)}$ = 0.0555]
Obs. reflections [$I > 2\sigma(I)$]	8752
T_{min}, T_{max}	0.3628, 1.0000
R_1, wR_2 indices (obs.)	R_1 = 0.0675, wR_2 = 0.1858
R_1, wR_2 indices (all)	R_1 = 0.0926, wR_2 = 0.1958
GOF on F^2	1.019

2.3. Powder X-ray diffraction

Powder X-ray diffraction (PXRD) pattern was collected on a MiniFlex 600 diffractometer using Cu-K_α radiation (λ = 1.540598 Å) at 30 kV and 15 mA. The simulated pattern of $[(Et_2)HDABH(Et_2)]_2Pb_5I_{14}{\cdot}2H_2O$ was derived from the Mercury Version 1.4 software.

2.4. UV–vis diffuse reflectance spectroscopy

Optical diffuse reflectance spectrum was measured on a PerkinElmer Lambda-950 UV/Vis/NIR spectrophotometer equipped with an integrating sphere attachment and $BaSO_4$ as reference. The optical diffuse reflectance spectrum was calculated from the reflection spectrum *via* the Kubelka–Munk function: $\alpha/S = (1 - R)^2/2R$, in which α is the absorption coefficient, S is the scattering coefficient and R is the reflectance.

Table 2
Selected bond distances for **1**.

Bond	Length (Å)	Bond	Length (Å)
Pb(1)-I(1)	3.003(2)	Pb(3)-I(7)	3.222(1)
Pb(1)-I(2)	3.142(2)	Pb(3)-I(4)#2	3.254(1)
Pb(1)-I(3)	3.201(2)	Pb(3)-I(4)	3.254(1)
Pb(1)-I(5)#1	3.223(2)	I(5)-Pb(1)#3	3.223(2)
Pb(1)-I(4)	3.396(2)	Pb(3)-I(7)#2	3.222(1)
Pb(2)-I(5)	3.082(2)	I(7)-Pb(2)#2	3.332(2)
Pb(2)-I(3)	3.165(2)	I(7)-Pb(2)#1	3.338(2)
Pb(2)-I(6)	3.217(2)	Pb(2)-I(7)#2	3.332(2)
Pb(2)-I(4)	3.249(2)	Pb(3)-I(6)#1	3.180(1)

Table 3
Selected bond angles for **1**.

Bond	Angles (°)	Bond	Angles (°)
I(4)-Pb(2)-I(7)#2	88.33(4)	I(1)-Pb(1)-I(2)	95.68(5)
I(5)-Pb(2)-I(7)#3	88.55(4)	I(1)-Pb(1)-I(3)	93.95(5)
I(6)#1-Pb(3)-I(4)#2	88.79(3)	I(2)-Pb(1)-I(3)	90.91(4)
I(6)#4-Pb(3)-I(4)#2	91.21(3)	I(1)-Pb(1)-I(5)#1	87.54(5)
I(7)#2-Pb(3)-I(4)#2	89.85(3)	I(2)-Pb(1)-I(5)#1	95.86(4)
I(7)-Pb(3)-I(4)#2	90.15(3)	I(6)-Pb(2)-I(7)#3	87.12(4)
I(6)#1-Pb(3)-I(4)	91.21(3)	I(1)-Pb(1)-I(4)	90.41(5)
I(6)#4-Pb(3)-I(4)	88.79(3)	I(6)#1-Pb(3)-I(7)#2	90.22(3)
I(7)#2-Pb(3)-I(4)	90.15(3)	I(3)-Pb(1)-I(4)	88.04(4)
I(7)-Pb(3)-I(4)	89.85(3)	I(5)#1-Pb(1)-I(4)	85.01(4)
Pb(2)-I(5)-Pb(1)#3	93.52(4)	I(5)-Pb(2)-I(3)	90.89(4)
Pb(3)#3-I(6)-Pb(2)	92.93(4)	I(5)-Pb(2)-I(6)	92.80(4)
Pb(3)-I(7)-Pb(2)#2	90.29(3)	I(3)-Pb(2)-I(6)	93.46(4)
Pb(3)-I(7)-Pb(2)#1	89.96(3)	I(5)-Pb(2)-I(4)	91.71(4)
Pb(2)#2-I(7)-Pb(2)#1	93.86(4)	I(3)-Pb(2)-I(4)	91.28(4)
Pb(2)-I(3)-Pb(1)	92.82(4)	I(4)-Pb(2)-I(7)#3	88.19(4)
Pb(2)-I(4)-Pb(3)	91.19(4)	I(7)#2-Pb(2)-I(7)#3	86.14(4)
Pb(2)-I(4)-Pb(1)	87.86(4)	I(3)-Pb(2)-I(7)#2	94.42(4)
Pb(3)-I(4)-Pb(1)	92.30(4)	I(6)-Pb(2)-I(7)#2	86.74(4)

Symmetry transformations used to generate equivalent atoms: #1: x + 1, y, z; #2: −x, −y + 1, −z + 1; #3 x-1, y, z; #4: −x−1, −y + 1, −z + 1.

2.5. Electronic conductivity measurement

The single crystal electrode was made using silver paste for **1**, and 50 μm diameter gold wires by placing the crystal between two electrodes. The temperature-dependent I–V curves were measured by KEITHLEY4200-SCS.

2.6. Humidity detection measurement

The crystals of compound **1** were ground with ethanol to form a suspension in mortar. The suspension was coated on an Al_2O_3 substrate loaded with interdigitated Ag-Pd electrodes by drop-casting method to form the sensing layer. Two 50 μm diameter gold wires were stuck to the two electrodes by silver paste. The humidity response measurement was performed by the reported instrument at room temperature [14]. The water vapor was generated by bubbling method. It took about 1.30 min to fulfil the quartz chamber when the gas constant flow was 600 mL min^{-1}. The bias on the device was 1.0 V and the current was recorded using Keithley 2602B Source meter.

3. Results and discussion

3.1. Structure description

The structure of **1** is composed of 1D $(Pb_5I_{14})^{4-}$ nanobelts, $[(Et_2)HDABH(Et_2)]^{2+}$ dications and water molecules. There are three crystallographically independent Pb atoms (Pb1, Pb2, Pb3) in the asymmetric unit, which are all situated in slightly distorted octahedral coordination environments. Five Pb atoms (Pb1, Pb2, Pb3, Pb1A, and PbA2) centered $[PbI_6]$ coordinated octahedra edge-share with each other to form a metal-halogen chain, with a width of 2.2 nm (Fig. 1a, S2). These five octahedral based chains extending to form a nanobelt along the *a* axis through edge sharing (Fig. 1b). The Pb—I bond distances fall in the range of 3.003 (2) to 3.396 (2) Å, and the I–Pb–I bond angles are ranging from 85.01 (4) to 95.86 (4)° (Tables 2 and 3). These values are similar to those of reported in the literatures [15]. Noteworthy, there are many structural types of reported lead halide anions have various structural types, including discrete 0D clusters like $(PbI_4)^{2-}$ [16], $(PbCl_6)^{4-}$ [17], $(Pb_3I_{10})^{4-}$ [18], $(Pb_7Cl_{31})^{17-}$ [19], $(Pb_{10}I_{28})^{8-}$ [20], $(Pb_{18}I_{44})^{8-}$ [21]; 1D chains such as $(PbI_3)^{-}$ [22], $(PbI_5)^{3-}$ [23], $(PbCl_5)^{3-}$ [24], $(Pb_2I_6)^{2-}$ [25], $(Pb_3I_{10})^{4-}$ [26]; 2D layers such as $(PbI_4)^{2-}$ [27], $(PbCl_4)^{2-}$ [28], $(PbCl_3)^{-}$ [17], $(Pb_4I_{18})^{10-}$ [29] as well as 3D $(Pb_7I_{18})^{4-}$, $(Pb_{21}Cl_{59})^{17-}$ frameworks [30]. The nanobelt structure in this work is rarely reported in the literature. Each 1D iodoplumbate nanobelt is encapsulated in a quadrate channel, which is formed by four $[(Et_2)HDABH(Et_2)]^{2+}$ cation columns stacking along the *a* axis (Fig. 1c). The $[(Et_2)HDABH(Et_2)]^{2+}$ dications interacts with two neighboring ones through weak face-to-face π···π stacking interactions between the aromatic rings with a distance of 3.882(1) Å (Fig. S3). The water molecules fill in the space of the structure, the closest I···O distance is 3.632(1) Å (I1···O1W), which exceeds the sums of relevant van der Waals radii (I···O = 3.50 Å), and suggests there is no halogen bonding interaction according to distance criteria.

3.2. Experimental band gap

Solid-state UV–Vis diffuse spectra of **1** calculated from the diffuse reflectance data by using the Kubelka–Munk function is plotted in Fig. 2. The absorption edge can be estimated as 2.72 eV for **1**, which is consistent with the yellow color of the crystal and also suggests that **1** has potential semiconductor properties. The absorption edge of compound **1** shows a blue shift compared to that of lead(II) iodide (2.30 eV), which may be due to the reduced structure dimension of iodoplumbate anion.

3.3. Electronic conductivity and humidity sensor

The temperature-dependent I–V curves for the single crystal of **1** using a two-terminal-probe direct current method along the extension direction of $(Pb_5I_{14})^{4-}$ nanobelts are shown in Fig. 3a. Since $(Pb_5I_{14})^{4-}$ nanobelts extended along the *a* axis, the I–V curves of the sample were measured along this direction. As shown in Fig. S5, the compound is stable after heating to 150 °C, the electronic conductivities were measured from 30 °C to 150 °C. As shown in Fig. 3a, the slope of the I–V curves gradually increases by raising the ambient temperature. The conductivity of **1** is about 4.75×10^{-9} S cm^{-1} at 30 °C, and increases to 8.52×10^{-7} S cm^{-1} at 150 °C in dry air. All of the values fall in the range of typical semiconductive materials, and are compared to reported haloplumbates(II) [8,11]. The conductivity of **1** linearly increases by reducing the value of 1/T demonstrating its semiconductive features. The activation energy (E_a) of **1** can be calculated by fitting the electrical conductivity data to the Arrhenius equation. As shown in Fig. 3b, the activation energy of **1** is calculated to be 0.59 eV from the least-squares fits of the slopes.

We found that the conductivity of **1** was 4.75×10^{-9} S cm^{-1} in dry air and 1.72×10^{-7} S cm^{-1} in 45% relative humidity (RH) at 30 °C. Therefore, the performance of **1** as an active component of a humidity sensor was investigated. The dynamic response-recovery current curve of compond **1** based humidity sensor was displayed in Fig. 4a. It shows good response and recovery to a broad range of RH from 30% to 90%. A baseline current (~10^{-13} A) was established under dry air flow. The electrical current fastly increases upon exposure to humid air, and then reaches a relatively stable value gradually. The current drops fast back to the baseline current when the gas reverting to dry air. Responses were calculated to reveal the sensing characteristics of the compound **1** under different moisture. The response of the sensor for detecting the humidity in this paper is defined as the ratio of resistance in dry gas and in humidity gas:

$$R_{response} = R_{dry}/R_{humidity} - 1 = I_{humidity}/I_{dry} - 1$$

Response reached up to > 4 orders of magnitude at 90% RH, which is comparable to other metal oxides and metal-organic frameworks (MOFs) based humidity sensors [31]. The repeating circles of compound **1** toward 80% RH are shown in Fig. 4b. The current changes of the sample revert to the original value in each circle, indicating good repeatability of the sensor. Response time is defined as the time taken by the sensor to attain 90% of the final saturation current change in

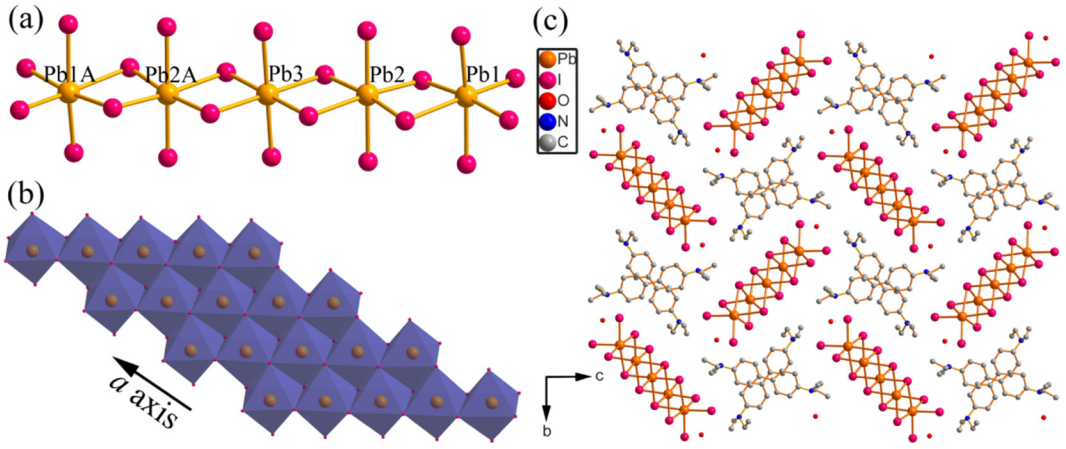

Fig. 1. (a) Five [PbI_6] octahedra chain in the iodoplumbate ion. (b) 1D nanobelt structure of the iodoplumbate ion in **1** extending along the *a* axis. (c) 3D packing of **1** along the *bc* plane with hydrogen atoms being omitted for clarity. Symmetry codes: A = 2 + x, y, z.

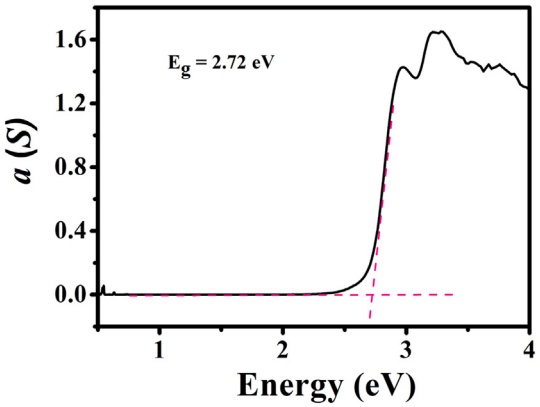

Fig. 2. Optical absorption spectrum for **1**.

humid air, while the recovery time is the time for the humidity sensor to recover to 10% of current change above the original current value in air. We calculated response and recovery time of the device at 90% RH. As shown in Fig. S7, response time for 90% RH was determined as *ca.* 115 s, whereas the corresponding recovery time is only 1.8 s. Its response time is shorter than graphene oxide [32] or silicon [33] based humidity sensor. It recovers faster than most of MOF based humidity sensors, even compared with carbon or metal oxides based sensors [34]. The adsorption/desorption behavior of water mainly formed on the surface of sensing materials, which makes H_2O molecules move through the materials easier, resulting in a rapid recovery speed [35]. All of these characteristics demonstrate its potential application in sensing of moisture.

It is widely recognized that water related conduction in sensing materials mainly occur as a surface mechanism. Resistance change along with humidity is dominated by the chemical and subsequently physical absorption of water molecules on the surface of compound **1**. Compound **1** is non-porous material, only the external surfaces are available for the adsorbed molecules, and the response value increases with the decreasing of size, as shown in Fig. S8. Thus, its humidity sensing responses mainly depend on outer surfaces of compound **1**. Reduced resistance might be ascribed to the reduced potential barrier and the activation energy of the sensing materials caused by water molecules and ionic functional hydroxyl groups adsorbed on grain surfaces, grain boundaries and interfaces between sensing materials and electrodes [36].

4. Conclusion

In summary, a novel inorganic-organic hybrid material, $[(Et_2)HDABH(Et_2)]_2Pb_5I_{14}{\cdot}2H_2O$, has been successfully synthesized and structurally characterized. The optical band gap was 2.72 eV, determined by the diffuse reflectance spectrum measurement. The application of electrically active haloplumbates as inorganic functional motif endowed the material with both typical semiconductive behavior and high electrical response to humidity (> 4 orders of magnitude resistance change at 90% RH). All characteristics demonstrate its potential application in humidity quantitatively detecting.

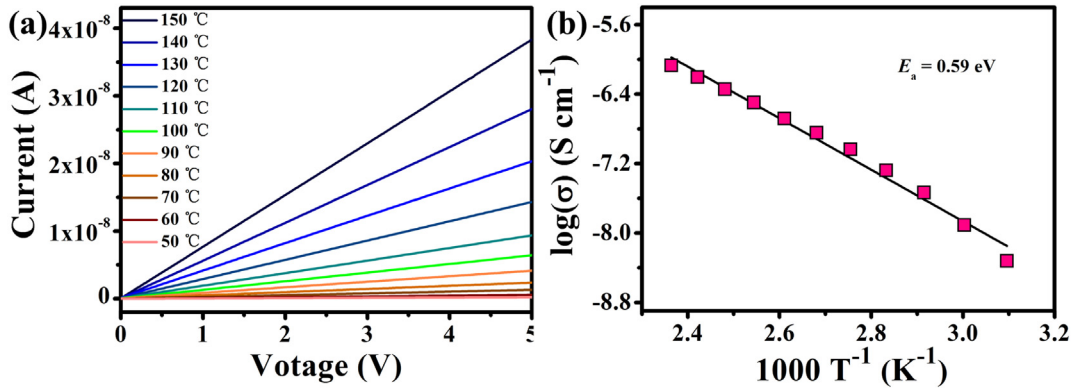

Fig. 3. (a) Temperature-dependent I–V curves for single crystal **1**. (b) Arrhenius plot of compound **1** at different temperatures.

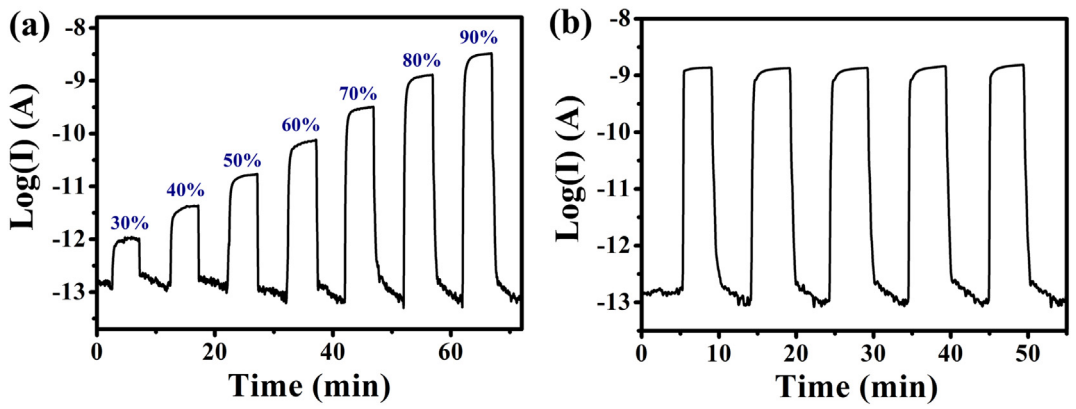

Fig. 4. (a) Current response of **1** to dry air and different RH (30%–90%) at room temperature; (b) The response and recovery under 80% RH for 5 cycles.

Acknowledgements

This work was supported by NSF of Fujian Province (2017J05034, 2016J06006, 2017J05094), Key Research Program of Frontier Science of CAS (QYZDB-SSW-SLH023), NSFC (21773245, 51602311, 21701189), Youth Innovation Promotion Association CAS, Scientific Research and Equipment Development Project, CAS (YZ201609).

Appendix A. Supplementary data

Supplementary data to this article can be found online at https://doi.org/10.1016/j.inoche.2018.05.002.

References

[1] P. Ruffieux, S.Y. Wang, B. Yang, C. Sánchez-Sánchez, J. Liu, T. Dienel, L. Talirz, P. Shinde, C.A. Pignedoli, D. Passerone, T. Dumslaff, X.L. Feng, K. Müllen, R. Fasel, Nature 531 (2016) 489–493.
[2] (a) J. Song, L. Xu, J. Li, J. Xue, Y. Dong, X. Li, H. Zeng, Adv. Mater. 28 (2016) 4861–4869;
(b) Z. Yuan, Y. Shu, Y. Tian, Y. Xin, B. Ma, Chem. Commun. 51 (2015) 16385–16388;
(c) A. Leblanc, N. Mercier, M. Allain, J. Dittmer, V. Fernandez, T. Pauporté, Angew. Chem. Int. Ed. 56 (2017) 16067–16072.
[3] Y. Zhang, W.Q. Liao, D.W. Fu, H.Y. Ye, Z.N. Chen, R.G. Xiong, J. Am. Chem. Soc. 137 (2015) 4928–4931.
[4] H.Y. Ye, Q. Zhou, X. Niu, W.Q. Liao, D.W. Fu, Y. Zhang, Y.M. You, J. Wang, Z.N. Chen, R.G. Xiong, J. Am. Chem. Soc. 137 (2015) 13148–13154.
[5] (a) A. Kojima, K. Teshima, Y. Shirai, T. Miyasaka, J. Am. Chem. Soc. 131 (2009) 6050–6051;
(b) G. Hodes, Science 342 (2013) 317–318;
(c) H. Si, Q. Liao, Z. Kang, Y. Ou, J. Meng, Y. Liu, Z. Zhang, Y. Zhang, Adv. Funct. Mater. 27 (2017) 1701804;
(d) Z.-K. Tang, Z.-F. Xu, D.-Y. Zhang, S.-X. Hu, W.-M. Lau, L.-M. Liu, Sci. Rep. 7 (2017) 7843.
[6] G.-C. Guo, Y.-G. Yao, K.-C. Wu, L. Wu, J.-S. Huang, Prog. Chem. 13 (2001) 151–155.
[7] C.C. Stoumpos, C.D. Malliakas, M.G. Kanatzidis, Inorg. Chem. 52 (2013) 9019–9038.
[8] G.-E. Wang, G. Xu, M.-S. Wang, L.-Z. Cai, W.-H. Li, G.-C. Guo, Chem. Sci. 6 (2015) 7222–7226.
[9] L.N. Li, Z.H. Sun, P. Wang, W.D. Hu, S.S. Wang, C.M. Ji, M.Ch. Hong, J.H. Luo, Angew. Chem. Int. Ed. 56 (2017) 12150–12154.
[10] D.B. Mitzi, C.A. Field, W.T.A. Harrison, A.M. Guloy, Nature 369 (1994) 467–469.
[11] G.-E. Wang, G. Xu, B.-W. Liu, M.-S. Wang, M.-S. Yao, G.-C. Guo, Angew. Chem. Int. Ed. 55 (2016) 514–518.
[12] X.-W. Lei, Ch.-Y. Yue, J.-Ch. Wei, R.-Q. Li, Y. Li, F.-Q. Mi, Dalton Trans. 45 (2016) 19389–19398.
[13] C.-K. Zhou, Y. Tian, M.-C. Wang, A. Rose, T. Besara, N.K. Doyle, Z. Yuan, J.C. Wang, R. Clark, Y.-Y. Hu, T. Siegrist, S.-C. Lin, B.-W. Ma, Angew. Chem. Int. Ed. 56 (2017) 9018–9022.
[14] M.-S. Yao, W.-X. Tang, G.-E. Wang, B. Nath, G. Xu, Adv. Mater. 28 (2016) 5229–5234.
[15] (a) D.B. Mitzi, Chem. Mater. 8 (1996) 791–800;
(b) Z. Tang, J. Guan, A.M. Guloy, J. Mater. Chem. 11 (2001) 479–482;
(c) H. Krautscheid, C. Lode, F. Vielsack, H. Vollmer, J. Chem. Soc. Dalton Trans. (7) (2001) 1099–1104.
[16] B.R. Vincent, K.N. Robertson, T.S. Cameron, O. Knop, Can. J. Chem. 65 (1987) 1042–1046.
[17] (a) L. Dobrzycki, K. Woźniak, CrystEngComm 10 (2008) 577–589;
(b) L. Dobrzycki, K. Woźniak, J. Mol. Struct. 921 (2009) 18–33.
[18] H. Krautscheid, F. Vielsack, J. Chem. Soc. Dalton Trans. 16 (1999) 2731–2735.
[19] D.G. Billing, A. Lemmerer, CrystEngComm 11 (2009) 1549–1562.
[20] A. Okrut, C. Feldmann, Z. Anorg. Allg. Chem. 632 (2006) 409–412.
[21] A. Cuna, I. Aguiar, A. Gancharov, M. Pérez, L. Fornaro, Cryst. Res. Technol. 39 (2004) 899–905.
[22] G.-E. Wang, M.-Sh. Wang, M.-J. Zhang, L.-Zh. Cai, B.-W. Liu, C.-J. Zhang, G.-C. Guo, J.-Sh. Huang, Inorg. Chem. Commun. 23 (2012) 137–141.
[23] (a) S. Wang, D.B. Mitzi, C.A. Feild, A. Guloy, J. Am. Chem. Soc. 117 (1995) 5297–5302;
(b) G.-N. Liu, J.-R. Shi, X.-J. Han, X. Zhang, K. Li, J. Li, T. Zhang, Q.-Sh. Liu, Zh.-W. Zhang, C.-Ch. Li, Dalton Trans. 44 (2015) 12561–12575.
[24] D.G. Billing, A. Lemmerer, CrystEngComm 8 (2006) 686–695.
[25] G.-E. Wang, G. Xu, M.-S. Wang, J. Sun, Z.-N. Xu, G.-C. Guo, J. Mater. Chem. 22 (2012) 16742–16744.
[26] A. Trigui, H. Abid, A. Mlayah, Y. Abid, Synth. Met. 162 (2012) 1731–1736.
[27] (a) J. Calabrese, N.L. Jones, R.L. Harlow, N. Herron, D.L. Thorn, Y. Wang, J. Am. Chem. Soc. 113 (1991) 2328–2330;
(b) X.-H. Zhu, N. Mercier, A. Riou, P. Blanchard, P. Frère, Chem. Commun. (2002) 2160–2161;
(c) N. Mercier, CrystEngComm 7 (2005) 429–432;
(d) D.G. Billing, A. Lemmerer, New J. Chem. 32 (2008) 1736–1746.
[28] (a) A.B. Corradi, A.M. Ferrari, G.C. Pellacani, A. Saccani, F. Sandrolini, P. Sgarabotto, Inorg. Chem. 38 (1999) 716–721;
(b) A.B. Corradi, A.M. Ferrari, L. Righi, P. Sgarabotto, Inorg. Chem. 40 (2001) 218–223.
[29] Z.-J. Zhang, G.-C. Guo, G. Xu, M.-L. Fu, J.-P. Zhou, J.-S. Huang, Inorg. Chem. 45 (2006) 10028–10030.
[30] Z.-J. Zhang, S.-C. Xiang, G.-C. Guo, G. Xu, M.-S. Wang, J.-P. Zhou, S.-P. Guo, J.-S. Huang, Angew. Chem. Int. Ed. 47 (2008) 4149–4152.
[31] (a) W. Xie, B. Liu, S. Xiao, H. Li, Y. Wang, D. Cai, D. Wang, L. Wang, Y. Liu, Q. Li, T. Wang, Sensor Actuat B-Chem. 215 (2015) 125–132;
(b) M. Tian, Z.-H. Fu, B. Nath, M.-S. Yao, RSC Adv. 6 (2016) 88991–88995;
(c) J.H. Huang, Y.H. He, M.-S. Yao, J. He, G. Xu, M. Zeller, Z. Xu, J. Mater. Chem. A 5 (2017) 16139–16143.
[32] X. Wang, Z. Xiong, Z. Liu, T. Zhang, Adv. Mater. 27 (2015) 1370–1375.
[33] Q. Kuang, C. Lao, Z.L. Wang, Z. Xie, L. Zheng, J. Am. Chem. Soc. 129 (2007) 6070–6071.
[34] (a) Y. Zhang, Y. Chen, Y. Zhang, H. Cong, B. Fu, S. Wen, S. Ruan, J. Nanopart. Res. 15 (2013) 2014;
(b) W.P. Chen, Z.G. Zhao, X.W. Liu, Z.X. Zhang, C.G. Suo, Sensors 9 (2009) 7431–7444.
[35] L. Wang, Y. He, J. Hu, Q. Qi, T. Zhang, Sensor Actuat B-Chem. 153 (2011) 460–464.
[36] X.-J. Lv, M.-S. Yao, G.-E. Wang, Y.-Z. Li, G. Xu, SCIENCE CHINA Chem. 60 (2017) 1197–1204.